Electronic Supplementary Information

Deep sulfur doping induces rapid electrochemical self-reconstruction of Ni-Fe hydroxide to drive water oxidation

Xiaoge Li[a]*, Jun Zhao[a], Jinhua Zhou[b], Qinchao Wang[a]*, Jie Han[a]*

[a] School of Chemistry and Chemical Engineering, Yangzhou University, Yangzhou 225002, Jiangsu Province, China

[b] School of Electronic and Information Engineering, Changshu Institute of Technology, Changshu 215500, China

Co-corresponding author:

xge_li@yzu.edu.cn, wangqinchao@yzu.edu.cn, hanjie@yzu.edu.cn

1. Experimental section

1.1. Chemicals

Hydrochloric acid (HCl, AR, Sinopharm Group Chemical Reagent Co. Ltd.), anhydrous ethanol (C_2H_5OH, AR, Shanghai Ling Feng Chemical Reagent Co., Ltd.), sodium hydroxide (NaOH, AR, Aladdin), ammonium persulfate ($(NH_4)_2S_2O_8$, AR, Shanghai Macklin Biochemical Co., Ltd.), sodium ascorbate ($C_6H_7O_6Na$, AR, Aladdin), nickel(Ⅱ) chloride hexahydrate ($NiCl_2{\cdot}6H_2O$, AR, Aladdin), Iron(III) chloride hexahydrate ($FeCl_3{\cdot}6H_2O$, AR, Shanghai Ling Feng Chemical Reagent Co., Ltd.), sodium thiosulfate pentahydrate ($Na_2S_2O_3{\cdot}5H_2O$, AR, Shanghai Macklin Biochemical Co., Ltd.), ruthenium(IV) oxide power (RuO_2, AR, Shanghai Macklin Biochemical Co., Ltd.), potassium hydroxide (KOH, ACS, Aladdin), and Cu foam (thickness: 0.5 mm) were used without further purification.

1.2. Synthesis of $Cu(OH)_2/Cu_2O$ nanowires array on Cu foam

All samples were prepared at normal temperature and pressure. The preparation of copper hydroxide underwent a typical chemical oxidation process, and the steps were as follows. The Cu foam (CF) was cut into rectangle with an area of 2.0 cm × 1.0 cm, and cleaned with hydrochloric acid solution (1 M) for 10 minutes. Subsequently, it was ultrasonically washed in anhydrous ethanol and deionized water for 15 minutes sequentially. The cleaned CF was immersed into 10 mL of an aqueous solution of 4 M NaOH and 0.2 M $(NH_4)_2S_2O_8$ for 25 min. Afterwards, CF was taken from the solution, washed with deionized water and anhydrous ethanol for several times, and dried in air. Finally, it can be clearly observed that a layer of blue material was formed on the surface of the CF, showing that the $Cu(OH)_2$ nanowires array has been successfully prepared.

In this step, the dried $Cu(OH)_2$ nanowires array was immersed in 10 mL of 5 M NaOH solution for 10 min to obtain $Cu(OH)_2/Cu_2O$ nanowires array. After that, the sample was taken out of the solution, rinsed several times with ethanol and deionized water, and dried in air. The freshly prepared $Cu(OH)_2/Cu_2O$ nanowires array was inserted in 10 mL of 0.1 M $C_6H_7O_6Na$ solution for 30 min. During this process, it can be found that $Cu(OH)_2/Cu_2O$ gradually change from blue to green.

1.3. Synthesis of S-$NiFe(OH)_x$ nanosheets around $Cu(OH)_2$ nanowires on CF

The synthesis of S-$NiFe(OH)_x$ catalyst was mainly divided into two steps. First, the 2 mL of 0.1 M $FeCl_3$ ethanol solution was dropped into 10 mL of 0.1 M $NiCl_2$ ethanol solution and mixed well, then the dried $Cu(OH)_2/Cu_2O$ nanowires array was fully immersed in this solution for 10 min. Afterwards, 10 mL of 1.0 M $Na_2S_2O_3$ solution was slowly dropped into that mixed solution. After standing for 10 min, $Cu(OH)_2/Cu_2O$ nanowires array was taken out of the mixed solution and washed several times with ethanol and deionized water, and dried at room temperature. Finally, the samples were directly used as the self-supported oxygen evolution reaction (OER) electrode.

The mass loading of the products growing on the CF is ~8.75 $mg{\cdot}cm^{-2}$ (including $Cu(OH)_2/Cu_2O$) for S-$NiFe(OH)_x$ electrode.

1.4. Synthesis of $NiFe(OH)_x$ nanosheets around $Cu(OH)_2$ nanowires on CF

This part was similar to the above procedure for the preparation of S-$NiFe(OH)_x$, except that the step of dropping 1 M $Na_2S_2O_3$ solution was removed.

1.5. Synthesis of S-$Ni(OH)_2$ and S-$Fe(OH)_3$ around $Cu(OH)_2$ nanowires on CF

This part was similar to the above procedure for the preparation of S-$NiFe(OH)_x$, except that $FeCl_3$ or $NiCl_2$ was absent.

1.6. Preparation of CF-RuO_2 electrode

In order to obtain the CF-RuO_2 electrode, a mixture of RuO_2 (5 mg), Nafion solution (10 μL), deionized water (500 μL) and anhydrous ethanol (500 μL) was ultrasounded for 20 min to disperse evenly. The well mixed solution was then dropped onto the cleaned CF and dried at room temperature. The amount of active substance was about 0.2 $mg{\cdot}cm^{-2}$.

1.7. Characterization

The surface morphology and nanostructure of the samples were visualized by scanning electron microscopy (SEM, S-4800) and transmission electron microscopy (TEM, Tecnai 12). The phases and components of materials were characterized by X-ray diffraction (XRD) on D8 Advance diffractometer. X-ray photoelecton spectroscopy (XPS) was conducted on a ESCALAB 250Xi XPS Microprobe. The high-resolution transmission electron microscope (HRTEM) images and energy dispersive X-ray spectroscopy (EDS) of the samples were acquired by Tecnai G2 F30 S-TWIN instrument.

1.8. Electrochemical measurements

All electrochemical performance tests in this work were carried out by Bio-logic VMP3 electrochemical workstation at room temperature. The standard three-electrode test system was used which consists of the as-prepared material as the working electrode, Hg/HgO as the reference electrode and graphite electrode as the counter electrode, and the electrolyte was 1.0 M KOH alkaline solution. At the same time, the measured potential used in this study needed to be converted to the reversible hydrogen electrode (RHE) potential based on the Nernst equation, and the specific equation is : $E_{RHE} = E_{Hg/HgO} + 0.059 \times pH + 0.098$. The catalyst was firstly activated by cyclic voltammetry (CV) until the curve remained stable. After obtaining a stable CV curve, the linear sweep voltammetry (LSV) was conducted from 0.924 to 1.624 V (*vs*. RHE) at a scan rate of 5 $mV \cdot s^{-1}$, and the corresponding Tafel slope were obtained through the conversion equation ($\eta = b \log |j| + a$, where η is overpotential, b refers to Tafel slope, and j stands for current density). The electrochemical double-layer capacitances (C_{dl}) of the samples were calculated via CV test at different scan rates of 10, 20, 30, 40 and 50 $mV \cdot s^{-1}$ in non-Faraday potential range (0.924 V-1.024 V *vs*. RHE) to facilitate the comparison of electrochemical surface area (ECSA). Electrochemical impedance spectroscopy (EIS) tests were also performed in the frequency range of 100 kHz-10 mHz using an amplitude of 10 mV with a set potential of 1.574 V (*vs*. RHE). In addition, the Faraday efficiency (FE) of OER was measured in a two-cavity electrolytic cell with RS-S-NiFe$(OH)_x$ as anode and graphite rod as cathode. The relevant equation is：

$$FE = \frac{V_{exp.}}{V_{the.}} = \frac{V_{exp.}}{\frac{VmQ}{nF}}$$

where V_{exp} stands for the volume of oxygen measured in the experiment, V_{the} for the theoretical volume of oxygen, V_m for the molar volume of gas (24.5 $L \cdot mol^{-1}$), Q for the amount of charge, n for the number of electron transfers and F for the Faraday constant (96,485 $C \cdot mol^{-1}$). Finally, the long-term stability of RS-S-NiFe$(OH)_x$ catalyst was evaluated by a continuous test for 36 h under a constant current density of 10 $mA \cdot cm^{-2}$. The polarization curves shown in this work were corrected with 85% *iR* compensation.

1.9. Calculational method

First-principles calculations are performed using the VASP software package based on the projected augmented wave (PAW) method within density function theory (DFT), and the spin-polarized calculation is turned on. The Perdew-Burke-Ernzerhof functional is used for the calculation of the exchange correlation interaction. Based on the results discussed in the previous literature, the U_{eff} values for Ni and Fe were set to 6.0 and 4.0 eV, respectively. During structural relaxation, convergence thresholds of 1×10^5 eV and -2×10^{-3} eV $Å^{-1}$ were adopted for the self-consistent energies and forces, respectively. In the calculation, the plane wave cutoff energy was set to 500 eV, and Monkhorst-Pack k-point mesh was 1×2×2 for 1×4×4 supercells.

2. Figures and tables

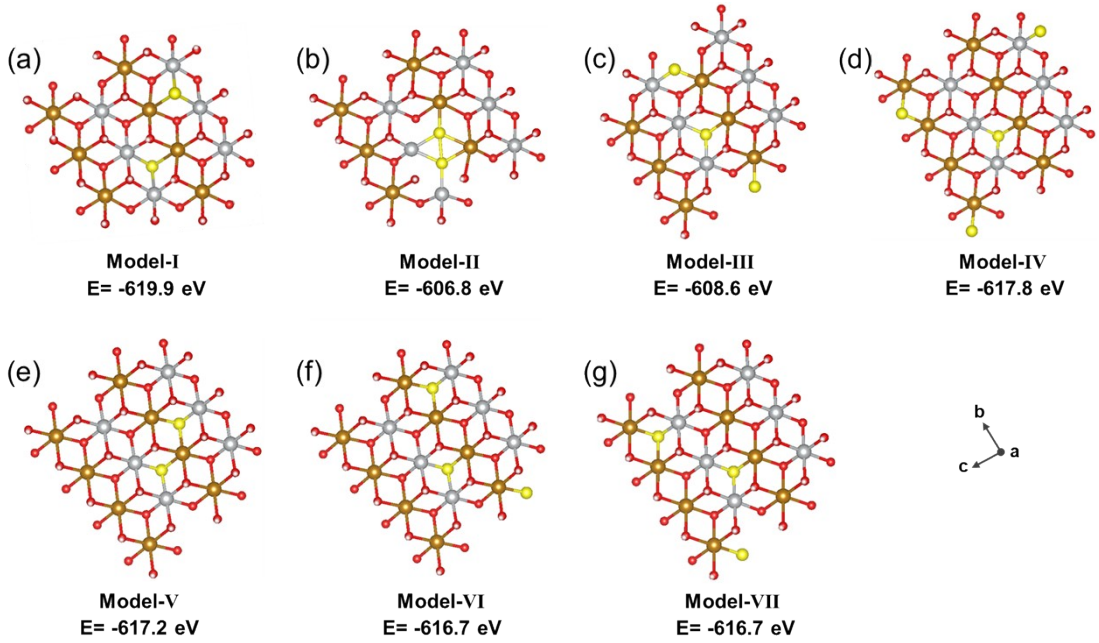

Fig. S1 (a-g) Possible structures and energies of sulfur-substituted oxygen models.

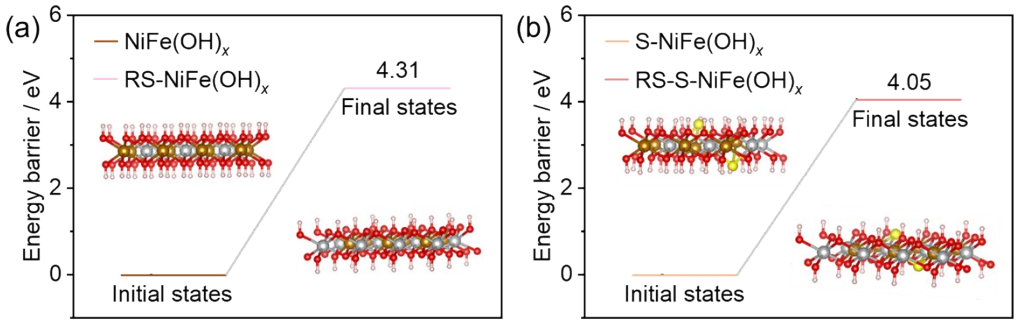

Fig. S2 The energy barrier for dehydrogenation.

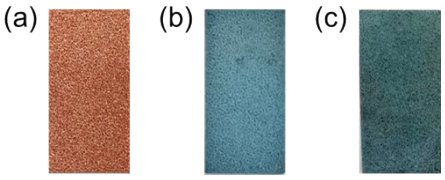

Fig. S3 Digital images of (a) CF, (b) $Cu(OH)_2$, (c) $Cu(OH)_2/Cu_2O$.

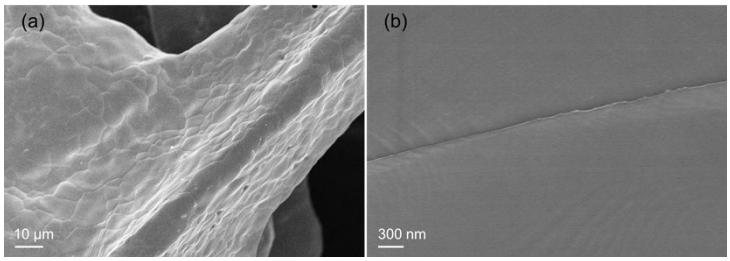

Fig. S4 SEM images of Cu foam under different magnifications.

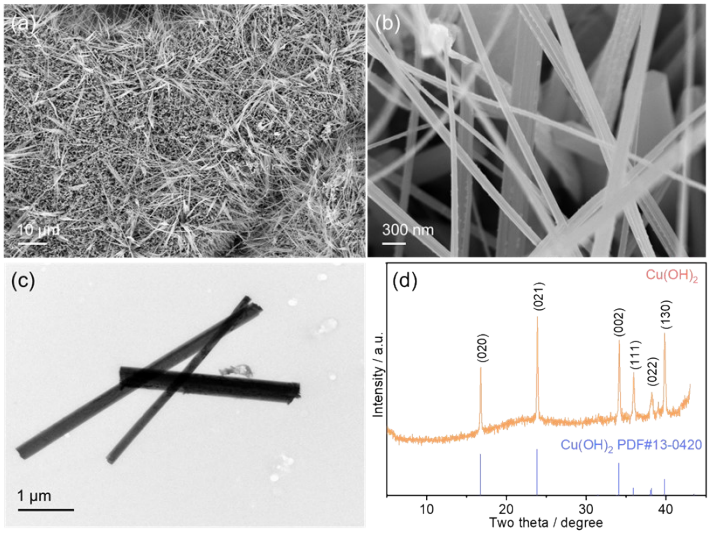

Fig. S5 (a-b) SEM images, (c) TEM image and (d) XRD pattern of $Cu(OH)_2$ nanowires.

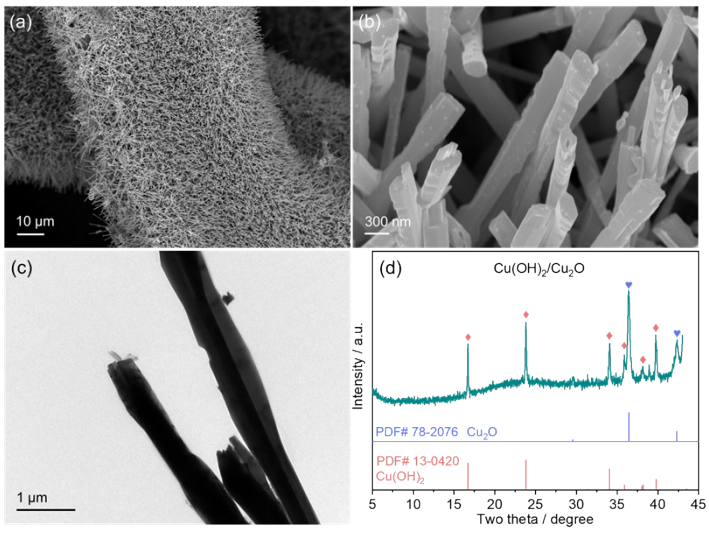

Fig. S6 (a-b) SEM images, (c) TEM image and (d) XRD pattern of $Cu(OH)_2/Cu_2O$ nanowires.

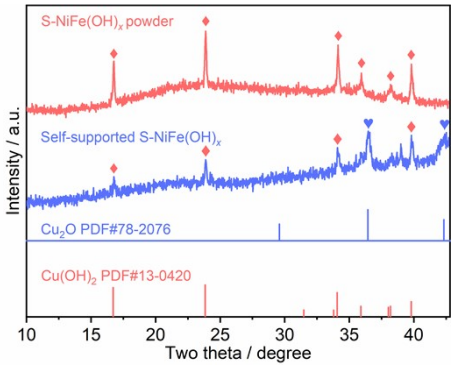

Fig. S7 XRD pattern of S-NiFe(OH)$_x$.

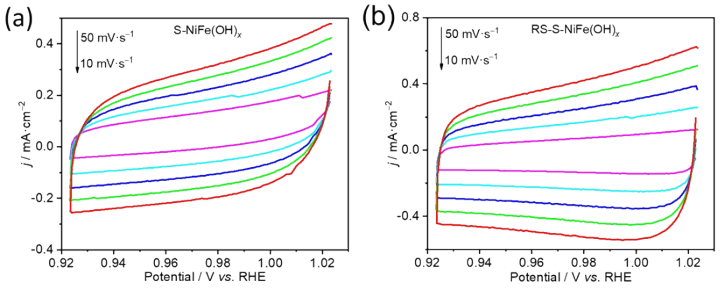

Fig. S8 CV curves of (a) S-NiFe(OH)$_x$ and (b) RS-S-NiFe(OH)$_x$ electrodes in non-Faradaic region at scan rates of 10, 20, 30, 40 and 50 mV·s^{-1} in 1.0 M KOH aqueous electrolyte.

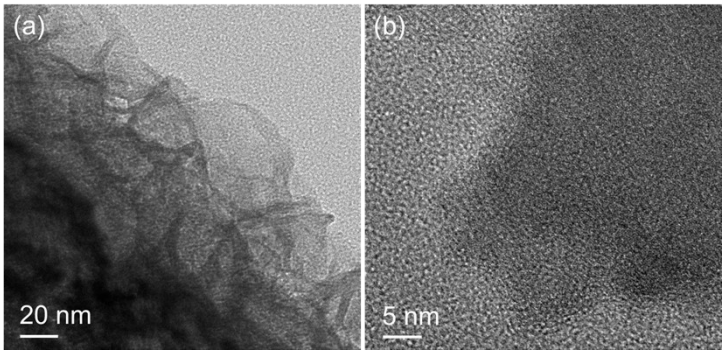

Fig. S9 (a) TEM and (b) HRTEM images of RS-S-NiFe(OH)$_x$.

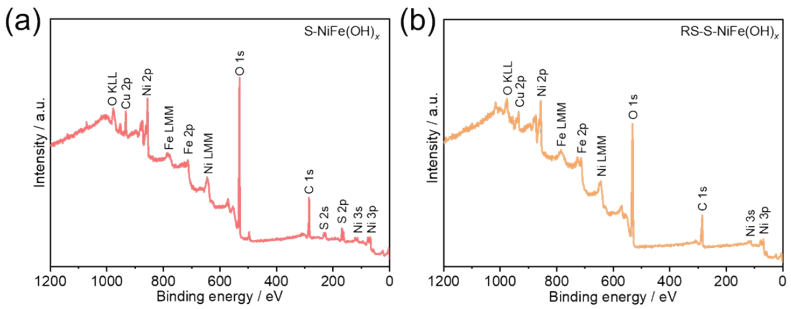

Fig. S10 XPS survey spectra of (a) S-NiFe(OH)$_x$ and (b) RS-S-NiFe(OH)$_x$.

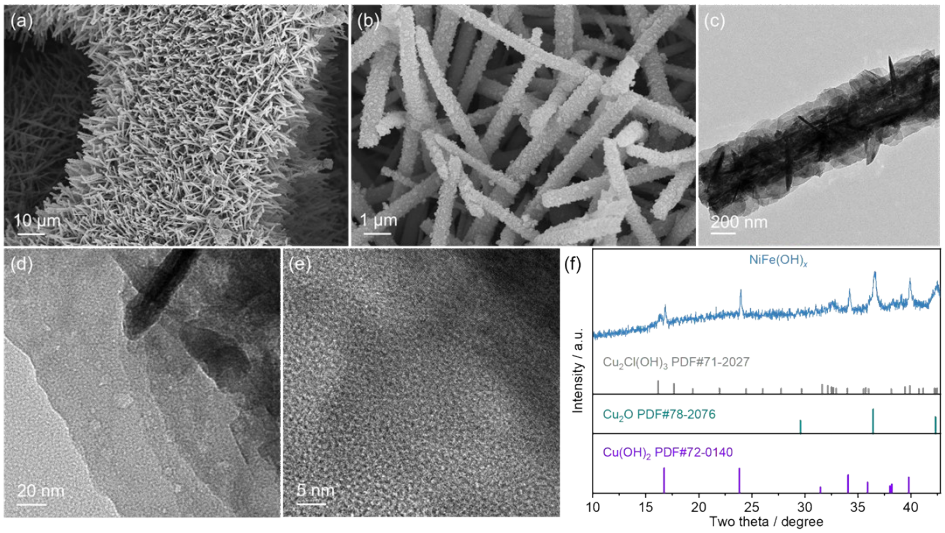

Fig. S11 (a-b) SEM, (c-d) TEM, (e) HRTEM images and (f) XRD pattern of NiFe(OH)$_x$.

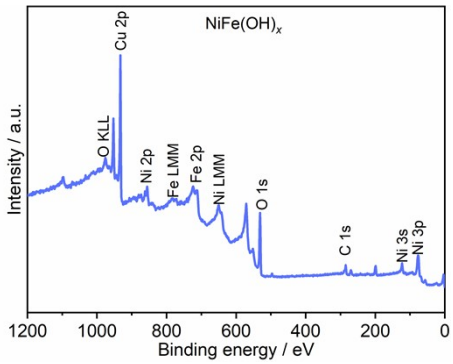

Fig. S12 XPS survey spectrum of NiFe(OH)$_x$.

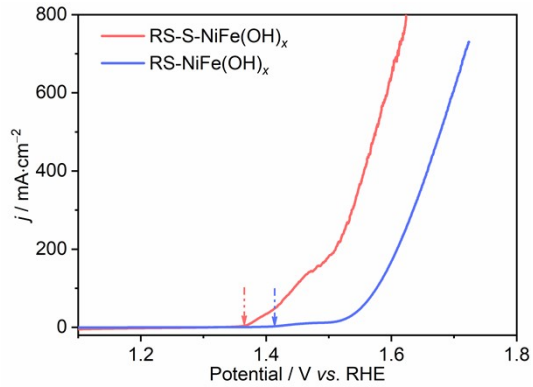

Fig. S13 *iR*-corrected OER polarization curves (1.10-1.72 V).

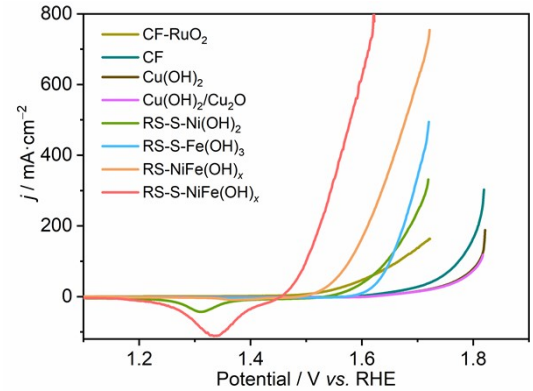

Fig. S14 *iR*-corrected OER polarization curves (1.83-1.20 V).

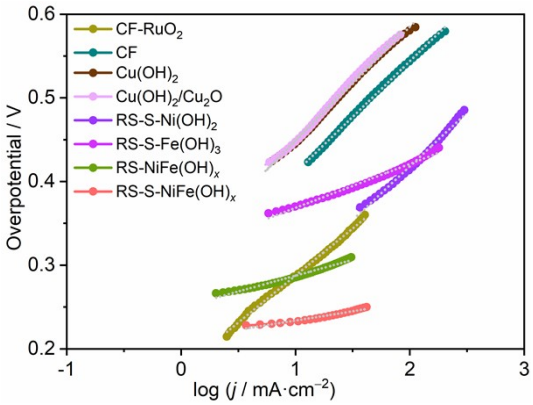

Fig. S15 Tafel plots calculated from corresponding OER polarization curves.

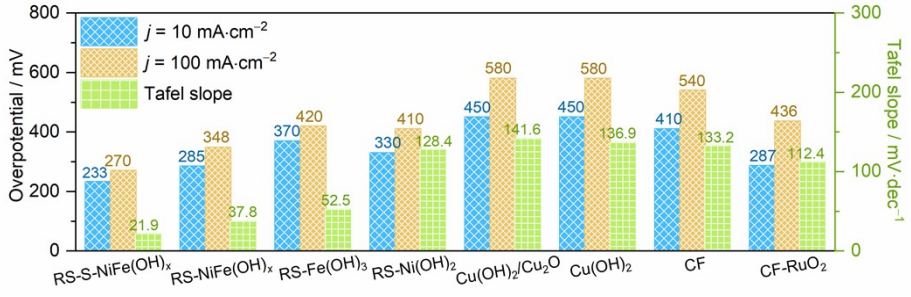

Fig. S16 Overpotentials required to achieve the current density of 10 and 100 mA·cm^{-2} and the Tafel slopes of all catalysts in this work.

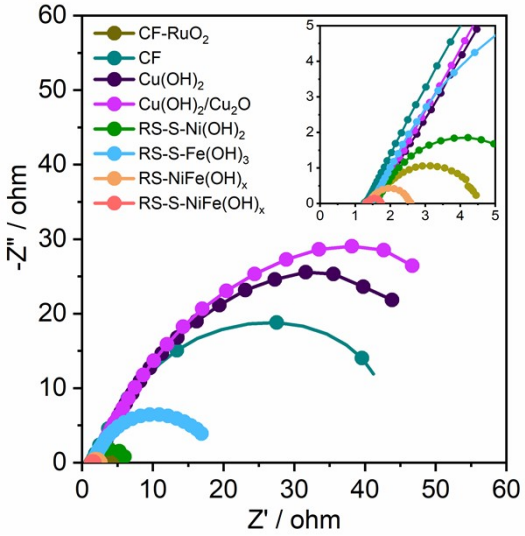

Fig. S17 Nyquist plots of all catalysts in this work.

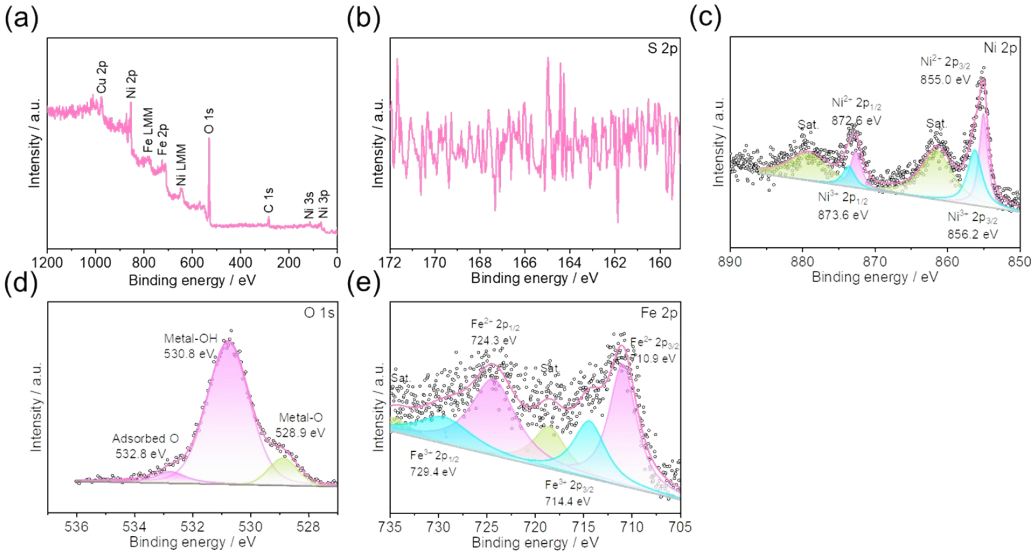

Fig. S18 (a) XPS survey spectrum, (b) S 2p, (c) Ni 2p, (d) O 1s and (e) Fe 2p spectra of RS-S-NiFe(OH)$_x$ after CP test for 36 h.

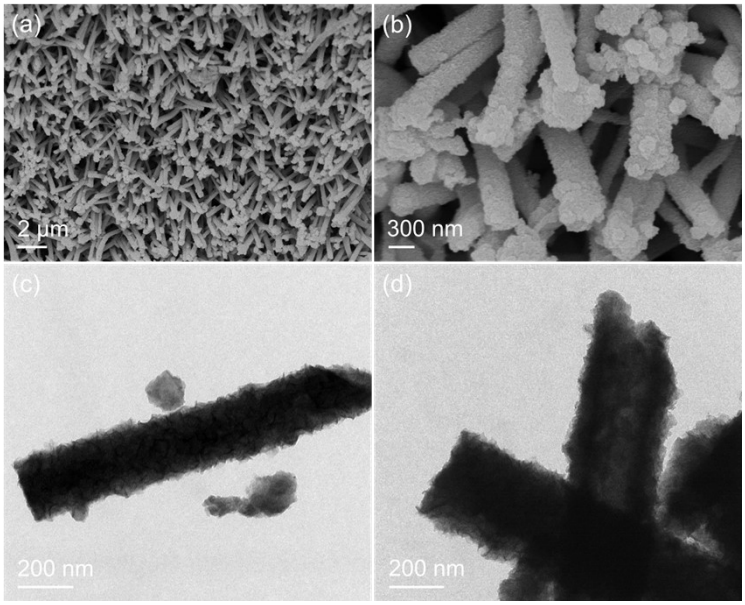

Fig. S19 (a-b) SEM and (c-d) TEM images of RS-S-NiFe(OH)$_x$ after CP test for 36 h.

Table S1 The charge transfer resistance values of all catalysts in this work.

Samples	RS-S-$NiFe(OH)_x$	RS-$NiFe(OH)_x$	RS-$Fe(OH)_3$	RS-$Ni(OH)_2$
R_{ct} (Ω)	0.43	1.27	15.46	4.56
Samples	**$Cu(OH)_2/Cu_2O$**	**$Cu(OH)_2$**	**CF**	**CF-RuO_2**
R_{ct} (Ω)	45.17	42.32	39.92	3.02

Table S2 Comparison of OER catalytic activity in 1.0 M KOH electrolyte between RS-S-$NiFe(OH)_x$ and recently reported self-supporting nickel-iron based catalysts.

Catalysts	Support	η_{10}[a] (mV)	η_{100}[b] (mV)	Tafel slpoe ($mV \cdot dec^{-1}$)	Reference
RS-S-$NiFe(OH)_x$	Cu foam	233	270	21.9	This work
NiFe-LDH/NF-3.5	Ni foam	249	303	49.8	Sustain. Mater. Technol., 2022, 34, e00508.
Fe-Ni_3S_2/FeNi	FeNi alloy foil	282	N.A.	54	Small, 2017, 13, 1604161.
$Ni_{18}Fe_{12}Al_{70}$	Ni foam	255	345	44	Angew. Chem. Int. Ed., 2023. 62, e202300800.
H-CoS_x@NiFe LDH/NF	Ni foam	250	312	49	Small, 2022, 18, 2200586.
FeNi@FeNiB-700	FeNi foam	272	399	136	J. Mater. Chem. A, 2019, 7, 19554.
NiFe-OOH_{ov}	Ni foam	270	N.A.	38	ACS Appl. Mater. Interfaces, 2021, 13, 55281.
Ni_3S_2@MoS_2/FeOOH/NF	NI foam	234	282	49	Appl. Catal. B Environ., 2019, 244, 1004.
δ-FeOOH NSs/NF	Ni foam	265	370	36	Adv. Mater. 2018, 30, 1803144.
FeP_2/NF	Ni foam	240	315	56	Adv. Funct. Mater. 2020, 30, 1907791.
CoFe-NA2/NF	Ni foam	250	363	69.9	J. Energy Chem., 2022, 65, 405.
NiFeP/NF	Ni foam	242	279	34	Appl. Catal. B Environ., 2021, 297, 120434.
Fe-Ni_3S_2/AF	FeNi foam	267	N.A.	36	Nano Res., 2021, 14, 4740.
NiFe LDH/NF-IH	NI foam	246	N.A.	46.65	Adv. Funct. Mater., 2021, 31, 2009580.
NFF-MOF	FeNi foam	250	N.A.	53	ACS Sustain. Chem. Eng., 2021, 9, 1826.
Pt_3Ni_1/Ni_xFe LDHs	Ni foam	265	N.A.	22.2	J. Mater. Chem. A, 2020, 8, 16355.

[a] The overpotential at the current density of 10 $mA \cdot cm^{-2}$.

[b] The overpotential at the current density of 100 $mA \cdot cm^{-2}$.